CONSTRAINTS ON DARK ENERGY MODELS FROM OBSERVATIONAL DATA

by

DATA MANIA

B.S., Tbilisi State University, Georgia, 2006
M.S., Ilia State University, Georgia, 2010

A THESIS

submitted in partial fulfillment of the
requirements for the degree

MASTER OF SCIENCE

Department of Physics
College of Arts and Sciences

KANSAS STATE UNIVERSITY
Manhattan, Kansas
2012

Approved by:

Major Professor
Bharat Ratra

Copyright

Data Mania

2012

Abstract

Recent observations in cosmology suggest that the universe is undergoing accelerating expansion. Mysterious component responsible for acceleration is called "Dark Energy" contributing to 70% of total energy density of the universe.

Simplest DE model is ΛCDM, where Einsteins cosmological constant plays role of the dark energy. Despite the fact that it is consistent with observational data, it leaves some important theoretical questions unanswered. To overcome these difficulties different Dark energy models are proposed. Two of these models XCDM parametrization and slow rolling scalar field model ϕCDM, along with "standard" ΛCDM are disscussed here, constraining their parameter set.

In this thesis we start with a general theoretical overview of basic ideas and distance measures in cosmology. In the following chapters we use H II starburst galaxy apparent magnitude versus redshift data from Siegel et al.(2005)[89] to constrain DE model parameters. These constraints are generally consistent with those derived using other data sets, but are not as restrictive as the tightest currently available constraints.

Also we constrain above mentioned cosmological models in light of 32 age measurements of passively evolving galaxies as a function of redshift and recent estimates of the product of the cosmic microwave background acoustic scale and the baryon acoustic oscillation peak scale.

Table of Contents

List of Figures

List of Tables

Acknowledgments

I am grateful to my supervisor, Dr. Bharat Ratra, who guiding my research and whose understanding and patience were invaluably helpful in my graduate studies. I am thankful to Dr. Larry Weaver, whose expertise and attitude towards physics, make me to desire to know more. Special thank goes to Dr. Glenn Horton-Smith, whose suggestions greatly helped me, when I was stuck because of programming related issues.

I am thankful to Omer Farooq, my roommate and colleague, for the valuable advices while writing the thesis, for helping me in research and in general.

Many thanks thanks to all people in K-State and around Manhattan because of whom I was enjoying my studies and my stay here.

Chapter 1

General Overview

1.1 Introduction

The universe is homogenous and isotropic in sufficiently large scales. This statement is known as **cosmological principle**[60] and it is a cornerstone on what the modern cosmology is based on. It simply means that we do not have special location and for any observer in any part of the cosmos a large scale picture of the universe will look the same. Also from observations it is known that our universe is expanding. Below we will try to give the minimal theoretical background necessary to understand the basics of the research outlined in the Chapter 3.

Expansion of the universe means that distance l between any two non-interacting (Not gravitationally bound) objects is increasing with time. That is

$$l(t) \propto a(t)$$

Where the dimensionless expansion parameter $a(t)$ or the scale factor is increasing function of time and it is independent of choice of the objects and reference frame in accordance with cosmological principle. Corresponding line element (Friedmann-Lemaître-Robertson-Walker metric) in time orthogonal coordinates[1] can be written as[60]

$$ds^2 = dt^2 - a(t)^2 dl^2 = dt^2 - a(t)^2(dx^2 + dy^2 + dz^2) \tag{1.1}$$

---

[1]That is we chose metric tensor components g_{00}=1 and $g_{0\alpha}$=0
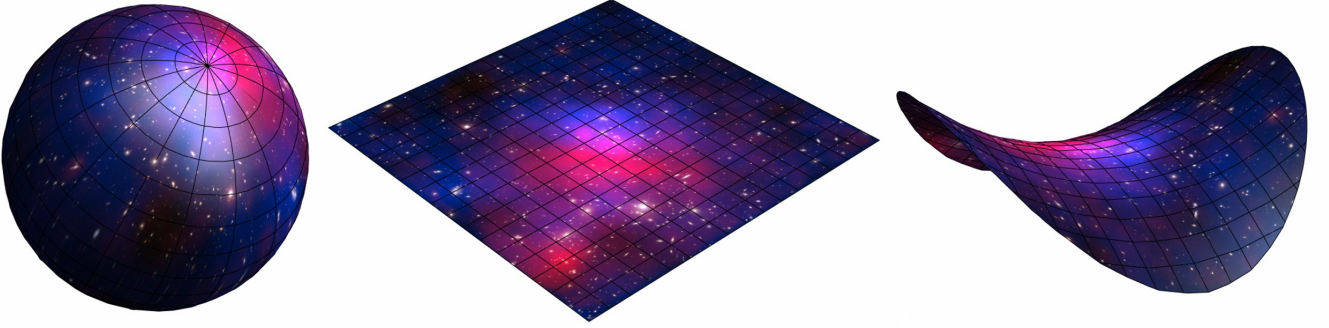
Figure 1.1: 2D Examples of positive, zero and negative curvature universes

Homogeneity and isotropy means that dl^2 part, for the fixed world time has a constant curvature[60]. We can think about 3D constant curvature surfaces like they are embedded in 4-dimensional Euclidean space, forming either 3D hypersphere of radius R or a pseudo-hypersphere in Minkowski space with imaginary radius. In simplest case curvature is 0, forming 3D analogy of a simple plain. In other words line element

$$dl^2 = dx^2 + dy^2 + dz^2 + dw^2$$

is subject to constraint

$$x^2 + y^2 + z^2 + w^2 = R^2 = \text{const}$$

Using 4D spherical coordinates

$$w = R\cos\chi$$
$$z = R\sin\chi\cos\theta$$
$$y = R\sin\chi\sin\theta\sin\varphi$$
$$x = R\sin\chi\sin\theta\cos\varphi$$

line element generalizes to

$$dl^2 = R^2[d\chi^2 + \sin^2\chi(d\theta^2 + \sin^2\theta d\varphi^2)] = R^2(d\chi^2 + \sin^2\chi d\Omega)$$

Where $d\Omega$ denotes the angular part of the metric. For negative curvature case substitution $w \to iw$, $R \to iR$ and $\chi \to -i\chi$ gives corresponding line element

$$dl^2 = R^2(d\chi^2 + \sinh^2\chi d\Omega)$$

In terms of radial variable $r = R \sin \chi$ line element becomes

$$dl^2 = \frac{dr^2}{1 - \kappa r^2} - r^2 d\Omega$$

Putting back in eqn. 1.1 we will get following form of FLRW metric[60]:

$$ds^2 = dt^2 - a(t)^2 R^2 (d\chi^2 + \sinh^2 \chi d\Omega) = dt^2 - a(t)^2 \left(\frac{dr^2}{1 - \kappa r^2} - r^2 d\Omega \right) \qquad (1.2)$$

where $\kappa \equiv 1/R^2$ is curvature parameter and when $\kappa = +1, 0, -1$ it defines closed, flat and open universes respectively.

Putting above metric in Einstein's equation,

$$G_{\mu\nu} \equiv R_{\mu\nu} - \frac{1}{2} g_{\mu\nu} R = 8\pi G T_{\mu\nu} + \Lambda g_{\mu\nu}$$

and referring to cosmological principle again, we can assume that on a large scale the universe can be considered as an isotropic and homogenous fluid. We can write energy-momentum tensor as:

$$T_{\mu\nu} = \text{diag}\left(\rho(t),\ p(t),\ p(t),\ p(t)\right)$$

We will get following equation for G_{00} component (where dot denotes time derivative)

$$3\frac{\dot{a}^2 + \kappa}{a^2} - \Lambda = 8\pi G \rho$$

taking trace of Einstein's equation gives the following (Or similarly we can use diagonal G_{ii} components)

$$-\frac{6\left(\kappa + \dot{a}^2 + a\ddot{a}\right)}{a^2} = 8\pi G(\rho - 3p)$$

Rearranging terms we will get two independent Friedmann's equations[60]:

$$\left(\frac{\dot{a}}{a}\right)^2 = \frac{8\pi G}{3}\rho + \frac{\Lambda}{3} - \frac{\kappa}{a^2}$$

$$\frac{\ddot{a}}{a} = -\frac{4\pi G}{3}\left(\rho + 3p\right) + \frac{\Lambda}{3}$$

(1.3)

Together with equation of state of fluid $p = p(\rho)$ the above equation closes set and defines behavior of the universe on a large scale. Taking time derivative from the first equation

3

and putting in the second (Or alternatively using that $T^{\nu}_{\mu;\nu} = 0$) yields energy conservation equation:

$$\dot{\rho} = -3\frac{\dot{a}}{a}(\rho + p) \tag{1.4}$$

Usually equation of state takes the form $p = w_i\rho$, where w_i is a constant equation of state parameter. Solving energy conservation for general species of w_i particles gives[60,77]

$$\rho(t) = \rho_0 \left(\frac{a_0}{a}\right)^{3(1+w_i)}$$

For non-relativistic matter $w_m = 0$ (cold dust do not exert pressure) and $\rho_m \propto a^{-3}$, for the radiation $w_\gamma = 1/3$ and $\rho_\gamma \propto a^{-4}$, for Λ $w_\Lambda = -1$ and $\rho_\Lambda \equiv \frac{\Lambda}{8\pi G} = $ const. If we have different species of particles, 1.4 holds separately for each set of them. Therefore total density $\rho(t)$ will be linear combination of corresponding densities. For example, Friedmann equation for non-relativistic matter, radiation, cosmological constant and curvature parameter can be written as:

$$\left(\frac{\dot{a}}{a}\right)^2 = A\frac{\rho_{m0}}{a^3} + B\frac{\rho_{\gamma0}}{a^4} + C\rho_\Lambda + D\frac{\rho_{\kappa0}}{a^2}$$

This equation defines evolution of the scale factor with given initial conditions. '

1.1.1 ΛCDM Model

Ratio $\frac{\dot{a}}{a}$ is known as a Hubble parameter. Present value of Hubble parameter is known as Hubble constant H_0. Taking into account that wave length scales as the scale factor $\lambda \sim a$ we can define redshift z

$$1 + z \equiv \frac{\lambda_{\text{obs}}}{\lambda_{\text{emi}}}$$

Denoting density parameters as follows:

$$\Omega_m = \frac{8\pi G\rho_0}{3H_0^2}, \ \Omega_\kappa = \frac{\kappa}{(H_0 a_0)^2}, \ \Omega_\Lambda = \frac{\Lambda}{3H_0^2}$$

we can rewrite Friedmann equation[2] in terms of redshifts and density parameters[60]

$$H(z)^2 = H_0^2(\Omega_\gamma(1 + z)^4 + \Omega_m(1 + z)^3 + \Omega_\kappa(1 + z)^2 + \Omega_\Lambda) \tag{1.5}$$

---

[2]as radiation contributing term dies quickly, we usually do not account for it in calculations

This equation describes the evolution of the Hubble parameter (and scale factor) in ΛCDM model.

1.2 Short summary of modern ideas in cosmology

According to current observations, we live in spatially-flat Universe that recently started accelerated expansion. Most cosmologists believe that acceleration is driven by dark energy, dominant component of the cosmological energy budget (for reviews of dark energy see[8,45,86,100] and references therein).[3]

In "standard" model of cosmology — the spatially-flat ΛCDM model[59] — Einstein's cosmological constant Λ plays role of the dark energy, contributing more than 70 % of total energy density parameter. Λ is followed by nonrelativistic cold dark matter (CDM) that is the next largest contributor (more than 20 %), and nonrelativistic baryons (around 5 %). For a review of the standard model see[76] and references therein. It is known that ΛCDM model is reasonably consistent with most observational constraints see, e.g.,[2,22,39,106] for early indications.[4]

However, in the framework of ΛCDM model some conceptual questions remain unanswered. E.g. measured cosmological constant energy scale is orders of magnitude smaller than we could expect from quantum field theory considerations. Another puzzle is the "coincidence problem". Cosmological constant energy density remains the same, but matter density decreases over time with cosmological expansion. It is unclear why we live at this special time, when nonrelativistic matter and dark energy densities are comparable.

These and possibly other puzzles could be solved, if we assume that the dark energy density was higher in the past and slowly decreased in time, thus remaining comparable to

---

[3] There exist alternative point of views and according to them accelerated expansion is just a sign that general relativity needs to be modified in order to correctly describe gravitation. see[24,38,100] and references therein. In this thesis we assume that general relativity adequately describes the gravitation on cosmological scales.

[4] The ΛCDM model assumes the "standard" CDM structure formation picture, which might be in some observational difficulty see, e.g.,[62,64].

the nonrelativistic matter density for a longer time[75]. Many such time-varying dark energy models have been proposed.[5] In this thesis, for illustrative purposes, we consider two dark energy models and one dark energy parametrization.

1.3 Alternative Dark Energy models

1.3.1 XCDM parametrization

In the ΛCDM model, time-independent dark energy — the cosmological constant — can be thought as a spatially homogeneous fluid with equation of state parameter[77] $w_\Lambda = p_\Lambda/\rho_\Lambda = -1$ (where p_Λ and ρ_Λ are the fluid pressure and energy density)

Now let's assume $\Lambda = 0$ in Einstein's equation. We can model dark energy as as a spatially homogeneous (X) fluid, but now with an equation of state parameter $w_X = \frac{p_X}{\rho_X}$, where $w_X(< -1/3)$[3] is an arbitrary constant and p_X and ρ_X are the pressure and energy density of the X-fluid. When $w_X = -1$ the XCDM parametrization reduces to the complete and consistent ΛCDM model. However, for any other value of $w_X(< -1/3)$, the XCDM parametrization is incomplete as it cannot describe spatial inhomogeneities see, e.g.[73,74]. For computational simplicity, here we study the XCDM parametrization in only the spatially-flat cosmological case. Putting corresponding density scaling, Hubble parameter takes the form

$$H(z, H_0, \mathbf{p}) = H_0\sqrt{\Omega_m(1+z)^3 + (1-\Omega_m)(1+z)^{3(1+w_X)}}.$$

1.3.2 ϕCDM Model

ϕCDM dark energy is modeled as a slow rolling inverse law potential scalar field[61]. Corresponding action is given by

$$S = \int \frac{1}{16\pi G}\left(g^{\mu\nu}\partial_\mu\phi\partial_\nu\phi - \frac{\kappa}{2G}\phi^{-\alpha}\right)\sqrt{-g}d^4x$$

---

[5] For recent discussions see, e.g.,[57,36,41,66,46,18,31], and references therein.

[3] Recall 1.3. To make $\ddot{a} > 0$ we need $w_X(< -1/3)$

where G is the Newtonian gravitational constant and $\alpha > 0$ is a free parameter (that determines κ). In spatially flat homogeneous case equation of motion is

$$\ddot{\phi} + 3H\dot{\phi} - \frac{\kappa\alpha}{2G}\phi^{-(\alpha+1)} = 0,$$

that with Hubble parameter

$$H(z) = H_0\sqrt{\Omega_m(1+z)^3 + \Omega_\phi(z)}.$$

and

$$\Omega_\phi(z) = \frac{1}{12H_0^2}\left(\dot{\phi}^2 + \frac{\kappa}{G}\phi^{-\alpha}\right)$$

defines coupled set of equation that determines evolution of the scalar field.

Stress-energy tensor takes the form

$$T_{00} = \rho = \frac{1}{32\pi G}\left(\dot{\phi}^2 + \frac{k}{G}\phi^{-\alpha}\right), \ T_{ii} = p = \frac{1}{32\pi G}\left(\dot{\phi}^2 - \frac{k}{G}\phi^{-\alpha}\right)$$

from where follows that equation of state parameter is

$$w(z) = \frac{\dot{\phi}^2 - k/G\phi^{-\alpha}}{\dot{\phi}^2 + k/G\phi^{-\alpha}}$$

When $\alpha \to 0$ model reduces to spatially flat ΛCDM case.

In early past when $\rho_\phi \ll \rho_{CDM}$ model accepts the solution,

$$\phi \propto a^{\frac{3(1+w_{CDM})}{a+2}}$$

and state parameter is

$$w_\phi = \frac{aw_{CDM} - 2}{a + 2}$$

Important property of this solution is that it is an attractor[77]. Wide range of initial conditions approach to it at some point.

In this model mentioned smallness and coincidence problem can be solved: ϕ field gradually decreases, remaining comparable to the non-relativistic matter density for a longer time[75]. It is worth to mention the scalar field with inverse power low potential is purely phenomenological classical field. And QFT of such field will be faced to usual problem of nonrenormazability.

Chapter 2

Distance measures in cosmology

2.1 Comoving distance, proper distance and coordinate distance

If we factor out expansion parameter, considering in that light travels in the radial directions at null geodesics, we will get expression for the comoving distance from eq. 1.2[60]

$$d_{co} = R\chi = \int_{t_e}^{t_0} \frac{dt'}{a(t')} = \int_{a_e}^{a_0} \frac{da}{a\dot{a}} = \frac{1}{a_0 H_0} \int_0^{z_e} \frac{dz}{E(z)} \tag{2.1}$$

Where t_e is photon emission time in observers frame, t_0 is present detection time and $E(z) = H(z)/H_0$ is dimensionless Hubble parameter[1]. Although it is integral over time, for any two distant galaxies moving with Hubble flow its value remains constant. Proper distance d at any fixed time is scale factor times comoving distance

$$d = a(t)d_{co}$$

Coordinate distance is $r = R\text{sinx}(\chi)$ from 1.2. Considering eq. 2.1 coordinate distance[2]

---

[1]Not to be confused: in general comoving distance $d_{co} \neq R\chi$ when direction is out of line of sight

[2]It should be noted that in the different literature this quantity is called differently, e.g. in Peebles[60] notation this quantity is *angular size distance*. This shouldn't confuse reader.
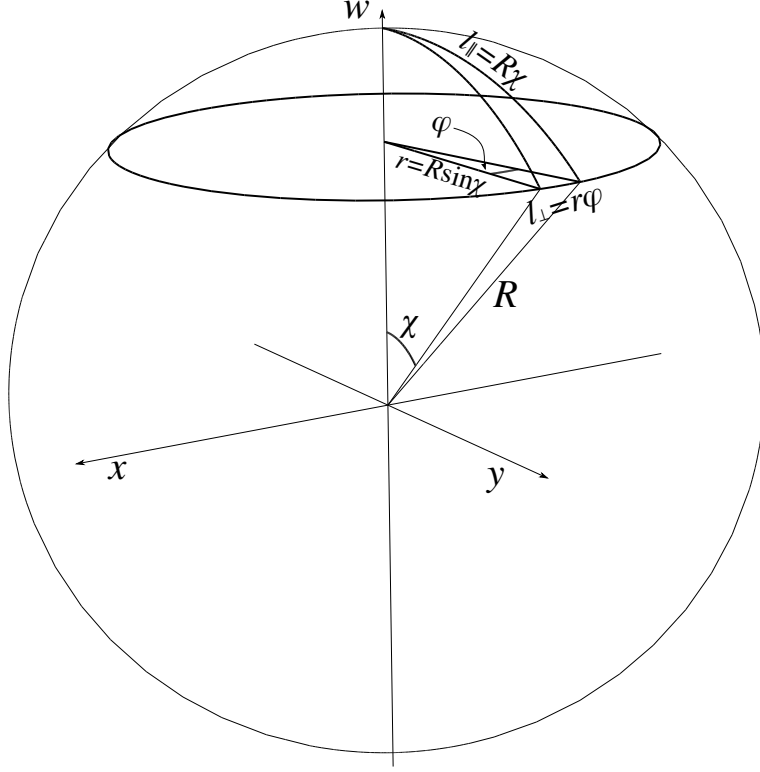
Figure 2.1: Diagram of 2D FLRW geometry

as a function of a redshift can be written as[60]

$$
r(z_e) =
\begin{cases}
\kappa^{-\frac{1}{2}} \sin \left(\dfrac{\kappa^{\frac{1}{2}}}{a_0 H_0} \displaystyle\int_0^{z_e} \dfrac{dz}{E(z)} \right) & \kappa > 0 \\[2em]
\dfrac{1}{a_0 H_0} \displaystyle\int_0^{z_e} \dfrac{dz}{E(z)} & \kappa = 0 \\[2em]
(-\kappa)^{-\frac{1}{2}} \sinh \left(\dfrac{(-\kappa)^{\frac{1}{2}}}{a_0 H_0} \displaystyle\int_0^{z_e} \dfrac{dz}{E(z)} \right) & \kappa < 0
\end{cases}
$$

It is useful to define dimensionless coordinate distance $y(z_e) \equiv a_0 H_0 r(z_e)$.

2.2 Angular diameter distance

Proper length $l_\perp$ subtended by an angle φ at a coordinate distance $r = R\mathrm{sinx}(\chi)$ is $l_\perp = ar\varphi \equiv d_A\varphi$ and defines angular diameter distance[60]

$$d_A = \frac{a_0 r}{1+z} = \frac{y(z)}{H_0(1+z)}$$

2.3 Luminosity distance

Luminosity distance is defined from the flux density luminosity relation, that is how far the object of known luminosity and measured flux will be if were in Euclidean space.

$$F = \frac{L}{4\pi d_L^2}$$

Let's assume a source emits dN photons in dt_e time interval. After photons traveled co-moving distance d_{co} they are spread over a surface area $S = 4\pi(a_0 r)^2$, time to collect the photons is $dt_0 = dt_e(1+z)$. And each emitted photon caries an energy $h\nu_e = h\nu_0(1+z)$. Observed apparent flux is:

$$F = \frac{h\nu_0}{S}\frac{dN}{dt_0} = \frac{h\nu_e}{4\pi a_0^2 r^2(1+z)^2}\frac{dN}{dt_e} = \frac{L}{4\pi(a_0 r(1+z))^2}$$

And for luminosity distance we will get[60]

$$d_L = a_0 r(1+z) = \frac{y(z)(1+z)}{H_0}$$

2.4 distance modulus

Apparent magnitude of an astronomical object is defined from the ratio of apparent flux of the object to some reference flux[77]

$$m = -2.5\log_{10}\left(\frac{F}{F_{\mathrm{ref}}}\right)$$

Absolute magnitude M is defined as a apparent magnitude, if the object were at 10 pc away. Difference between them is known as distance modulus and can be expressed as[60]:

$$\mu \equiv m - M = -2.5\log_{10}\left(\frac{F}{F_{10\mathrm{pc}}}\right) = 5\log_{10}\left(\frac{d_L}{10\mathrm{pc}}\right)$$

2.5 Age & lookback time

We can write rewrite Hubble's relation to get expression for time evolution

$$t = \int_0^a \frac{da}{aH} = \int_z^\infty \frac{dz}{(1+z)H(z)} = \int_0^{(1+z)^{-1}} \frac{dy}{yH(y)} \qquad (2.2)$$

Lookback time is defined as a difference between present time and time at particular redshift[60]. That is

$$t_L = \int_0^\infty \frac{dz}{(1+z)H(z)} - \int_z^\infty \frac{dz}{(1+z)H(z)} = \int_0^z \frac{dz}{(1+z)H(z)}$$

Chapter 3

Constraints on Dark Energy models

3.1 Cosmological observations

Observational data available today convincingly indicate that the Universe expansion is accelerating. The evidence of accelerated expansion comes mainly form three types of data: supernova Type Ia (SNIa) apparent magnitude versus redshift measurements see, e.g.,[3,35,37,101]; cosmic microwave background (CMB) anisotropy data see, e.g.,[42,43,47,72] combined with low estimates of the cosmological matter density see, e.g,[15]; and, baryon acoustic oscillation (BAO) peak length scale estimates see, e.g.,[7,63,82,103]. However, errors of these data are still very large and they do not allow sufficient discrimination between the ΛCDM model and the two simple time-varying dark energy models discussed in this thesis.

There are two main reasons to consider additional data sets. First of all, it's important to compare above results to the ones derived from other data. If there is significant difference, that could indicate that we used observationally inconsistent model, or it could mean the one of the data sets had an undetected systematic error. Both of the results would be important. But if the constraints from the new and the old data are consistent, then a joint analysis of all the data could produce constraints that are significantly tighter, allowing as a possible result discrimination between constant and time varying dark energy models.

Other data that have recently been used to constrain dark energy models include strong gravitational lensing measurements e.g.,[6,13,44,109], angular size as a function of redshift obser-

vations e.g.,[9,14,34], Hubble parameter as a function of redshift measurements e.g.,[40,58,78,80,88], galaxy cluster gas mass fraction data e.g.,[2,30,81,96], and large-scale structure observations e.g.,[5,10,11,23,54].

These data are less restrictive than those derived from the SNeIa, CMB and BAO data. However, they produce compatible constraints, thus supporting the models with accelerating expansion of the universe. But ambiguity still remains, because the observations are unable do discriminate between these different dark energy models. For instance, although available data hint cosmological constant is time-independent, they are still unable to rule out time-varying dark energy. To achieve this goal, the better quality data sets are required.

It is anticipated that future space missions will result in significantly more and better SNeIa, BAO, and CMB anisotropy data see, e.g.,[4,71,84,104]. A complementary approach is to develop cosmological tests that make use of different sets of objects. Recent examples include the lookback time test e.g.,[21,67] and the gamma-ray burst luminosity versus redshft test see, e.g.[87,102,107]. Gamma-ray bursts, in particular, are very luminous and can be seen to much higher redshifts than the SNeIa. Therefore, they could be used as the probes for an earlier cosmological epoch.

H II starburst galaxies also can be used as standardizable candles[51,53,95], because of the correlation between their velocity dispersion, H_β luminosity, and metallicity[50,52,94]. These galaxies also can be seen to redshifts exceeding 3.

In this thesis in the section 3.3 we use H II galaxy data from[89] to constrain parameters of the three dark energy models mentioned above. Plionis et al.[686970] have used the Siegel et al.[89] data to constrain the XCDM parametrization. Here we also constrain parameters of ΛCDM and ϕCDM cosmological models. We also derive constraints on the parameters of these models and the XCDM parametrization from a joint analysis of the Siegel et al.[89] H II galaxy data and the Percival et al.[63] BAO peak length scale measurements.

In the following section 3.4 we combine distance data with low and high-redshift time measurements to constrain accelerating cosmologies. In particular, we use age measurements

of 32 passively evolving galaxies[90] (in the range $0.117 \leq z \leq 1.845$) to constrain mentioned dark energy models. In order to better constrain the parameter spaces of these models, we combine the age-z data with a recent estimate of the ratio of the CMB acoustic scale ℓ_A and the baryonic acoustic oscillation (BAO) peak, the so-called CMB/BAO ratio[91].

3.2 Data analysis

Let's assume we have n independent measurements of observable y_i at known redshifts z_i. The measurement is assumed to be Gaussian with mean $f(z_i, \mathbf{p})$ (from model) and known variance σ_i. Our goal is to constrain parameter set $\mathbf{p}$ of cosmological models of our interest. First we build χ^2 function[55]

$$\chi^2 = \sum_{i=1}^{n} \frac{(y_i - f(z_i, \mathbf{p}))^2}{\sigma_i^2}$$

Minimizing the χ^2 with respect to $\mathbf{p}$ we can find the best fit least square estimator of model parameters $\tilde{\mathbf{p}}$. In our calculations models depend on two parameters. In this case, $\chi^2(\mathbf{p}) = \chi^2(\tilde{\mathbf{p}}) + 2.30$, $\chi^2(\mathbf{p}) = \chi^2(\tilde{\mathbf{p}}) + 6.17$, $\chi^2(\mathbf{p}) = \chi^2(\tilde{\mathbf{p}}) + 11.8$ describe 1, 2 and 3 standard deviation contours in 2 dimensional parameter space $\mathbf{p}$.

Let's assume f in model depends not only on parameters of our interest, but also on nuisance parameters ν, and its values are known with limited accuracy. If we have some estimated prior distribution for ν (for example, if ν is one parameter one can assume that it is Gaussian distributed with some variance σ_ν), we can build posterior likelihood function that will depend on $\chi^2(\mathbf{p})$ only[55]

$$\mathcal{L}(\mathbf{p}) = \int \mathcal{L}(\mathbf{p}, \nu) \pi(\nu) \mathrm{d}\nu$$

where $\mathcal{L}(\mathbf{p}, \nu) \equiv e^{-\frac{\chi^2(\mathbf{p}, \nu)}{2}}$ is a prior likelihood, and $\pi(\nu)$ is a prior distribution of the ν parameter. Maximizing $L(\mathbf{p})$, or similarly minimizing $\tilde{\chi}^2 = -2\ln(L(\mathbf{p}))$ we can estimate best point and calculate $N\sigma$ contours as described above.

When we have different set of independent observables, for example a_i and corresponding

$f_a(z_i, \mathbf{p})$ and b_i and $\bar{f}_b(z_k, \mathbf{p})$, we can build likelihood function

$$\mathcal{L} = \mathcal{L}_a \mathcal{L}_b$$

Or corresponding χ^2

$$\chi^2 = \chi_a^2 + \chi_b^2 = -2\ln(\mathcal{L}_a) - 2\ln(\mathcal{L}_b)$$

and constrain joint parameters.

The following section is based on Ref.[48]

3.3 Constraints from H II galaxy apparent magnitude data

3.3.1 H II galaxy data analysis

To constrain cosmological parameters, we use the 13 $\mu_{\mathrm{obs}}(z_i)$ measurements of[89], listed in Table 3.1. We minimize

$$\chi^2_{\mathrm{HII}}(H_0, \mathbf{p}) = \sum_{i=1}^{13} \frac{[\mu_{\mathrm{obs}}(z_i) - \mu_{\mathrm{pred}}(z_i, H_0, \mathbf{p})]^2}{\sigma_i^2}. \qquad (3.1)$$

Here $\mu_{\mathrm{obs}}(z_i)$ is measured and $\mu_{\mathrm{pred}}(z_i, H_0, \mathbf{p})$ is predicted distance modulus in the model under consideration at the same z_i redshift. σ_i is the average of the upper and lower error bars listed in Table 3.1.

The Siegel et al.[89] (The data itself is derived from[28,65]) measurements listed in Table 3.1 are computed from

$$\mu_{\mathrm{obs}} = 2.5 \log \left(\frac{\sigma^5}{F_{H\beta}} \right) - 2.5 \log \left(\frac{O}{H} \right) - A_{H\beta} + Z_0 \qquad (3.2)$$

where $F_{H\beta}$ and $A_{H\beta}$ are the H_β flux and extinction and O/H is a metallicity. Following Plionis et al.[69], for the zero point magnitude we use $Z_0 = -26.60$, we take Hubble constant value $H_0 = 73$ km s^{-1} Mpc^{-1} (and do not account for the associated uncertainty), and also exclude two H II galaxies (Q1700-MD103 and SSA22a-MD41) that show signs of a considerable rotational velocity component[29].

The χ^2_{HII} minimum χ^2_{min} defines best fit parameter set $\mathbf{p}_*$. Contours enclosed by $\chi^2 = \chi^2_{\mathrm{min}} + \Delta\chi^2$ with $\Delta\chi^2 = 2.30$, $\Delta\chi^2 = 6.17$, and $\Delta\chi^2 = 11.8$, defines 1σ, 2σ, and 3σ confidence intervals respectively. The H II galaxy data constraints on cosmological parameters of the three models are shown in Figs. 3.1. Our results are in good agreement with[69] for the XCDM parametrization (compare our top right Fig. 3.1 and their Fig. 10). The small differences arise from the fact that in our analysis gravitational lensing effects are ignored and

Table 3.1: [89] H II starburst galaxy distance moduli and uncertainties

Galaxy	z	$\mu_{\rm obs} \pm \sigma$
Q0201-B13	2.17	$47.49^{+2.10}_{-3.43}$
Q1623-BX432	2.18	$45.45^{+1.97}_{-3.07}$
Q1623-MD107	2.54	$44.82^{+0.31}_{-1.58}$
Q1700-BX717	2.44	$46.64^{+0.31}_{-1.58}$
CDFa C1	3.11	$45.77^{+0.31}_{-1.58}$
Q0347-383 C5	3.23	$47.12^{+0.44}_{-0.32}$
B2 0902+343 C12	3.39	$46.96^{+0.71}_{-0.81}$
Q1422+231 D81	3.10	$48.81^{+0.38}_{-0.40}$
SSA22a-MD46	3.09	$46.76^{+0.56}_{-0.51}$
SSA22a-D3	3.07	$49.71^{+0.43}_{-0.41}$
DSF2237+116a C2	3.32	$47.73^{+0.25}_{-0.25}$
B2 0902+343 C6	3.09	$45.22^{+1.38}_{-1.76}$
MS1512-CB58	2.73	$47.49^{+1.22}_{-1.57}$

also average distance moduli uncertainties are used rather than specially weighted sigmas. Small uncertainties of H_0 are ignored in both analyses; It's insignificant for our illustrative purposes here, but should be considered in an analysis of improved near-future H II galaxy data.

The H II galaxy data constraints in Figs. 3.1 are not as restrictive as those originating from SNeIa, BAO, or CMB anistropy data. They are, however, comparable to those from Hubble parameter observations see[17] and references therein or lookback time observations see[79] and references therein, and somewhat more restrictive than angular diameter distance constraints see[16] and references therein and gamma-ray burst luminosity distance ones see[83] and references therein. We again note that uncertainties in H_0 are not accounted in our analysis, therefore making H II galaxy constraints more restrictive than they really are. However, constraining power of near-future H II galaxy is clearly shown in our analysis.

3.3.2 Joint constraints from SNeIa, BAO and H II galaxy data

We use the SCP Union2.1 compilation of redshift versus distance modulus relation (580 points)[93] for the SNeIa analysis . We minimize the function

$$\chi^2_{\text{SN}} = (\Delta\boldsymbol{\mu})^T C^{-1} \Delta\boldsymbol{\mu}$$

where $\Delta\boldsymbol{\mu}$ is a vector consisting of differences $\Delta\mu_i = \mu_{\text{obs}}(z_i) - \mu_{\text{pred}}(z_i, H_0, \mathbf{p})$, the Hubble constant value used is $H_0 = 73$ km s^{-1} Mpc^{-1}, and C is the covariance matrix. The SNeIa data constraint contours are shown in Figs. 3.2. For the BAO data constraints, we follow the method of Percival et al.[63]. With $D_V(z) = [(1+z)^2 d_A^2 cz/H(z)]^{1/3}$ (where d_A is angular diameter distance),[63] measure

$$\bar{D}_V(0.275) = (1104 \pm 30) \left(\frac{\Omega_b h^2}{0.02273}\right)^{-0.134} \left(\frac{\Omega_m h^2}{0.1326}\right)^{-0.255} \text{Mpc.} \tag{3.3}$$

We construct $\chi^2_{\text{BAO}} = (\bar{D}_V - D_V(0.275, H_0, \mathbf{p}))^2/\sigma^2_{\bar{D}_V}$ and use this to build the likelihood estimator $\mathcal{L}_{\text{BAO}}$ with a Gaussian prior of $\mathbf{\Omega_m h^2} = 0.1326 \pm 0.0063$, and neglect the error for $\Omega_b h^2$ as WMAP5 data constrains it to 0.5 %[42]

$$\mathcal{L}_{\text{BAO}}(\mathbf{p}) = \int e^{-\frac{(\Omega_m h^2 - \mathbf{\Omega_m h^2})^2}{2\sigma^2}} e^{-\frac{\chi^2_{BAO}}{2}} \text{d}(\Omega_m h^2) \bigg/ \int e^{-\frac{(\Omega_m h^2 - \mathbf{\Omega_m h^2})^2}{2\sigma^2}} \text{d}(\Omega_m h^2) \tag{3.4}$$

The BAO data constraint contours are shown in Figs. 3.3.

To derive joint H II galaxy and SNeIa (Figs. 3.2); H II and BAO (Figs. 3.3); and the combined HII, SNeIa and BAO constraints (Figs. 3.4) we maximize the products of likelihoods $\mathcal{L}(\mathbf{p}) = \mathcal{L}_{\text{HII}}\mathcal{L}_{\text{SN}}$, $\mathcal{L}(\mathbf{p}) = \mathcal{L}_{\text{HII}}\mathcal{L}_{\text{BAO}}$ and $\mathcal{L}(\mathbf{p}) = \mathcal{L}_{\text{HII}}\mathcal{L}_{\text{SN}}\mathcal{L}_{\text{BAO}}$ respectively to get the best fit set of parameters $\mathbf{p}_*$, where $\mathcal{L}_{\text{SN}} = e^{-\chi^2_{\text{SN}}/2}$ and $\mathcal{L}_{\text{HII}} = e^{-\chi^2_{\text{HII}}/2}$. The 1, 2, and 3σ contours defined as points where the likelihood equals $e^{-2.30/2}$, $e^{-6.17/2}$, and $e^{-11.8/2}$ of the maximum likelihood value. For comparison we have given SNIa and BAO data only constraints in Figs. 3.4. It can be inferred from these figures, future improved H II data set can well complement SNeIa and BAO contours. Clearly, constraints tighten even when currently available H II galaxy data is added to SNeIa or BAO data and to their combination.

H II galaxy data itself is not yet of good enough quality and in the above analyses we are forced to ignore uncertainties on the Hubble constant as we already noted above. Therefore, contours in the figures appear to be tighter, than they really are.

3.3.3 Summary on H II constraints

Constraints from starburst galaxy luminosity distance data of Siegel et al.[89] used in our analysis are consistent with other available data sets. However, they are not as restrictive as SNeIa, BAO, and CMB anisotropy data constraints.

The H II data given in Siegel et al.[89] are preliminary H II data. We expect that near future space missions will significantly improve H II galaxy data quality. These data will complement other data sets and will be very useful to discriminate and constrain parameters of different cosmological models.

The following section is based on Ref.[21]

3.4 Cosmological constraints from age-redshift relation

3.4.1 The age-redshift test

The total age of a given object (e.g., galaxies) from observational point of view at redshift z is given by $t^{\mathrm{obs}}(z_i) = t_G(z_i) + \tau$, where where $t_G(z_i)$ is the estimated age of oldest stellar population in the object and τ is the incubation time or delay factor, which accounts our ignorance for the time period from the beginning of structure formation in the Universe until the formation time of the object of interest. For age-z analysis we use age estimates of 32 old passive galaxies 3.2 distributed over the redshift interval $0.117 \leq z \leq 1.845$ ([90]) as listed in Table 1 of[79], and assume a 12% one standard deviation uncertainty on the age measurements. The total sample is composed of three sub-samples: 10 field early-type galaxies from[97–99], whose ages were obtained by using the SPEED models of Jimenez et al. (2004); 20 red galaxies from the publicly released Gemini Deep Deep Survey (GDDS), whose integrated light is fully dominated by evolved stars[1,49]; and the 2 radio galaxies LBDS 53W091 and LBDS 53W069 ([27,56,92]). The GDDS data seem to indicate that star formation was consisted of single burst with duration less than 0.1 Gyr and in some cases burst duration is consistent with 0 Gyr[49]. That means that galaxies have been evolving passively since the initial burst of star formation.

We build the likelihood function $\mathcal{L} \propto [\exp -\chi^2_{age}(z; \mathbf{p}, \tau)/2]$ from

$$\chi^2_{age}(H_0, \tau, \mathbf{p}) = \sum_{i=1}^{32} \frac{[t(z_i, \mathbf{p}) - t_G(z_i) - \tau]^2}{\sigma^2_{t_{G,i}}} \,, \tag{3.5}$$

where $\sigma^2_{t_{G,i}}$ stands for the uncertainties on the age measurements of galaxy sample. It should be noted that in principle there must be a different τ_i for each object in the sample because galaxies form at different epochs. However, considering that we do not know the formation redshift for the particular objects, we assume a uniform delay factor τ that we treat as a

"nuisance" parameter and marginalize over it to get the posterior lakilihood function

$$\mathcal{L}(z; \mathbf{p}) \propto \int \exp\left[-\frac{1}{2}\chi^2_{age}(z; \mathbf{p}, \tau)\right] d\tau = \sqrt{\frac{\pi}{2C}} \exp\left[-\frac{1}{2}\left(A - \frac{B^2}{C}\right)\right] \text{erfc}\left(-\frac{B}{\sqrt{2C}}\right),$$

(3.6)

where,

$$A = \sum_{i=1}^{32} \frac{[t(z_i, \mathbf{p}) - t_G(z_i)]^2}{\sigma^2_{t_{G,i}}}, \quad B = \sum_{i=1}^{32} \frac{t(z_i, \mathbf{p}) - t_G(z_i)}{\sigma^2_{t_{G,i}}}, \quad C = \sum_{i=1}^{32} \frac{1}{\sigma^2_{t_{G,i}}}.$$

Similarly, we also numerically marginalize over the present value of the Hubble constant $H_0 = 74.2 \pm 3.6$ km s^{-1} Mpc^{-1} with the Gaussian prior[1].

3.4.2   CMB/BAO ratio

CMB and baryon oscillations data provide two main inputs involving acoustic oscillations. Commonly used quantities to constrain cosmological models are CMB shift parameter $\mathcal{R}$ and BAO parameter $\mathcal{A}$. However, use of these quantities is questionable for nonstandard cosmologies, because they are obtained in the context of extended XCDM parametrization (see, e.g.[26]).[2]

Here, following[91], we use a more model-independent constraint derived from the product of the CMB acoustic scale $\ell_A = \pi d_A(z_*)/r_s(z_*)$ and the measurement of the ratio of the sound horizon scale at the drag epoch and the BAO dilation scale, $r_s(z_d)/D_V(z_{\text{BAO}})$ [$d_A(z_*)$ is the comoving angular-diameter distance to recombination and $r_s(z_*)$ is the comoving sound horizon at decoupling]. By combining the ratio $r_s(z_d = 1020)/r_s(z_* = 1090) = 1.044 \pm 0.019$ ([42]) with the measurements of $r_s(z_d)/D_V(z_{\text{BAO}})$ at $z_{\text{BAO}} = 0.20$ and 0.35 from Percival et al.[63], Sollerman et al.[91] found (with one standard deviation error bars)

$$d_A(z_*)/D_V(0.2) = 17.55 \pm 0.65$$

---

[1]A variant of this test uses both measurements of the Hubble parameter as a function of redshift (see, e.g.[25,32,33,78,80,105,108]) and lookback time measurements built from estimates of the total age of the Universe[12,19,20,67,79,82]).

[2]For the BAO parameter $\mathcal{A}$, for instance, it is implicitly assumed that the evolution of matter density perturbations during the matter-dominated era must be similar to the ΛCDM case and also that the comoving distance to the horizon at the time of equilibrium between matter and radiation energy densities must scale with $(\Omega_m H_0^2)^{-1}$.

$$d_A(z_*)/D_V(0.35) = 10.10 \pm 0.38 \ ,$$

which we use in our analyses together with the age-z data. The correlations in the measurements are accounted by following[91].

3.4.3   Summary on Age-z test

To constrain parameters of 3 cosmological models, in the above analysis we used time (age-z) and distance (CMB/BAO) data. Our main results are shown in the figures 3.5 and figures 3.6 where age-z data and age-z plus CMB/BAO data contours are given respectively. Age-z data contours are not very restrictive, but combining them with CMB/BAO data puts tighter constraints on cosmological parameters. Particularly, in case of ΛCDM model (Fig.3.6 top left panel) orthogonality of contours for age-z and CMB/BAO data results tight parameter constraints when used together (see, e.g.,[67,79]).

Our results are generally consistent with those of SNeIa plus CMB/BAO data analysis (see, e.g.,[91]). Although age-z data are not able yet to discriminate between different cosmological models, the future improved set of age measurements expected to be very useful to put tighter bounds on cosmological models.

Table 3.2: Ages of 32 passively evolving galaxies and uncertainties

Redshift	Age	Uncertainty
0.1171	10.2	1.2
0.1174	10	1
0.222	9	0.9
0.2311	9	0.9
0.3559	7.6	0.76
0.452	6.8	0.68
0.575	7	0.7
0.644	6	0.6
0.676	6	0.6
0.833	6	0.6
0.836	5.8	0.58
0.922	5.5	0.55
1.179	4.6	0.46
1.222	3.5	0.35
1.224	4.3	0.43
1.225	3.5	0.35
1.226	3.5	0.35
1.34	3.4	0.34
1.38	3.5	0.35
1.383	3.5	0.35
1.396	3.6	0.36
1.43	3.2	0.32
1.45	3.2	0.32
1.488	3	0.3
1.49	3.6	0.36
1.493	3.2	0.32
1.51	2.8	0.28
1.55	3	0.3
1.576	2.5	0.25
1.642	3	0.3
1.725	2.6	0.26
1.845	2.5	0.25
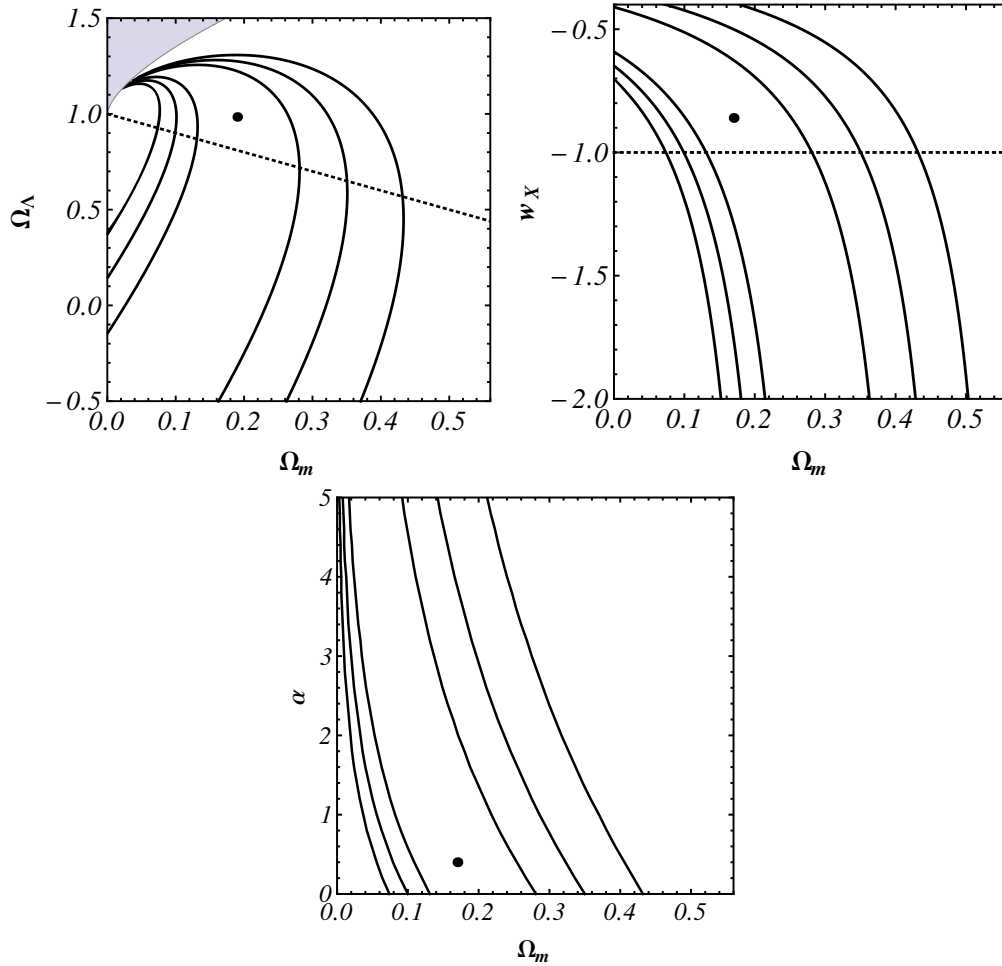
Figure 3.1: *Top left.* H II galaxy data 1, 2, and 3σ confidence level contours in the $(\Omega_m, \Omega_\Lambda)$ plane for the ΛCDM model. The dotted line corresponds to the spatially-flat ΛCDM case and the shaded area in the upper left hand corner is the part of parameter space without a big bang. The best-fit point with $\chi^2_{\min} = 53.3$ is indicated by the solid black circle at $\Omega_m = 0.19$ and $\Omega_\Lambda = 0.98$.

Top right. H II galaxy data 1, 2, and 3σ confidence level contours in the (Ω_m, w_X) plane for the spatially-flat XCDM parametrization. The dotted line corresponds to the spatially-flat ΛCDM case. The best-fit point with $\chi^2_{\min} = 53.3$ is indicated by the solid black circle at $\Omega_m = 0.17$ and $w_X = -0.86$.

Bottom. H II galaxy data 1, 2, and 3σ confidence level contours in the (Ω_m, α) plane for the spatially-flat ϕCDM model. $\alpha = 0$ corresponds to the spatially-flat ΛCDM case. The best-fit point with $\chi^2_{\min} = 53.3$ is indicated by the solid black circle at $\Omega_m = 0.17$ and $\alpha = 0.39$.

24
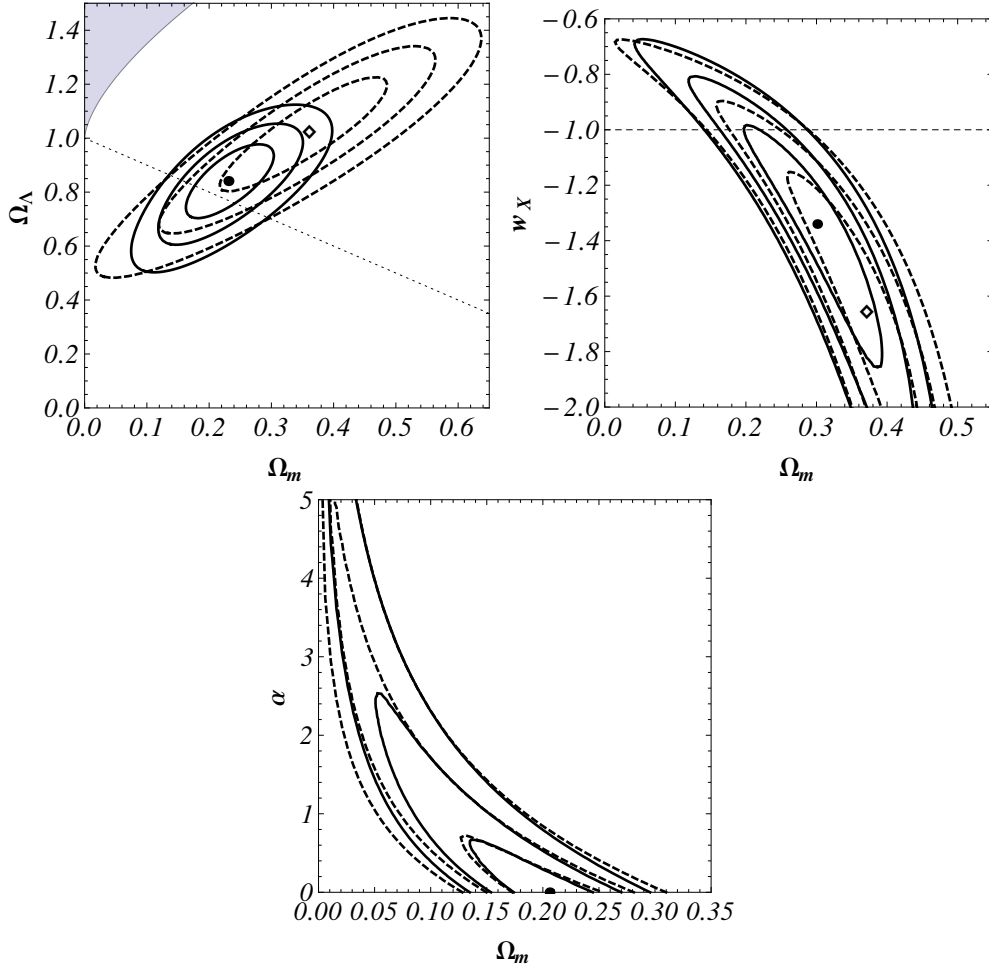
Figure 3.2: *Top left.* Joint H II galaxy and SNeIa data (solid lines) and SNeIa data only (dashed lines) 1, 2, and 3σ confidence level contours in the $(\Omega_m, \Omega_\Lambda)$ plane for the ΛCDM model. The best-fit point for the first case with $-2\log(\mathcal{L}_{\max}) = 610.4$ is indicated by the solid black circle at $\Omega_m = 0.23$ and $\Omega_\Lambda = 0.84$ and for the second $-2\log(\mathcal{L}_{\max}) = 555.9$ is indicated as a diamond at $\Omega_m = 0.36$ and $\Omega_\Lambda = 1.03$.
Top right. Joint H II galaxy and SNeIa data (solid lines) and SNeIa data only (dashed lines) 1, 2, and 3σ confidence level contours in the (Ω_m, w_X) plane for the spatially-flat XCDM parametrization. The best-fit point for the first case with $-2\log(\mathcal{L}_{\max}) = 608.7$ is indicated by the solid black circle at $\Omega_m = 0.30$ and $w_x = -1.34$ and for the second $-2\log(\mathcal{L}_{\max}) = 553.1$ is indicated as a diamond at $\Omega_m = 0.37$ and $w_x = -1.65$.
Joint H II galaxy and SNeIa data (solid lines) and SNeIa data only (dashed lines) 1, 2, and 3σ confidence level contours in the (Ω_m, α) plane for the spatially-flat ϕCDM model The best-fit point for the first case with $-2\log(\mathcal{L}_{\max}) = 610.7$ and for the second $-2\log(\mathcal{L}_{\max}) = 557.4$ is indicated by the solid black circle at $\Omega_m = 0.21$ and $\alpha = 0$.
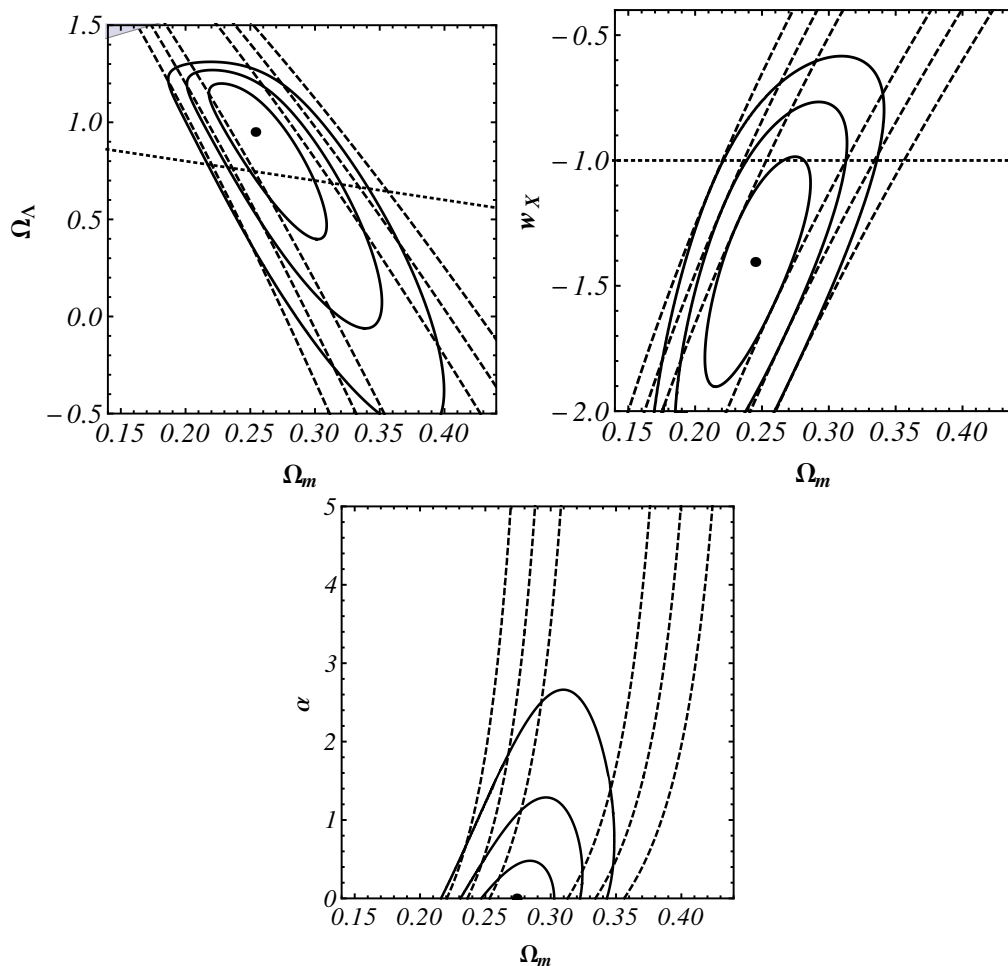
Figure 3.3: *Top left.* Joint H II galaxy and BAO data (solid lines) and BAO data only (dashed lines) 1, 2, and 3σ confidence level contours in the $(\Omega_m, \Omega_\Lambda)$ plane for the ΛCDM model. The best-fit point with $-2\log(\mathcal{L}_{\max}) = 55.2$ is indicated by the solid black circle at $\Omega_m = 0.25$ and $\Omega_\Lambda = 0.95$.
Top right. Joint H II galaxy and BAO data (solid lines) and BAO data only (dashed lines) 1, 2, and 3σ confidence level contours in the (Ω_m, w_X) plane for the spatially-flat XCDM parametrization. The best-fit point with $-2\log(\mathcal{L}_{\max}) = 53.5$ is indicated by the solid black circle at $\Omega_m = 0.25$ and $w_x = -1.41$.
Bottom. Joint H II galaxy and BAO data (solid lines) and BAO data only (dashed lines) 1, 2, and 3σ confidence level contours in the (Ω_m, α) plane for the spatially-flat ϕCDM model. The best-fit point with $-2\log(\mathcal{L}_{\max}) = 55.6$ is indicated by the solid black circle at $\Omega_m = 0.27$ and $\alpha = 0$.

26
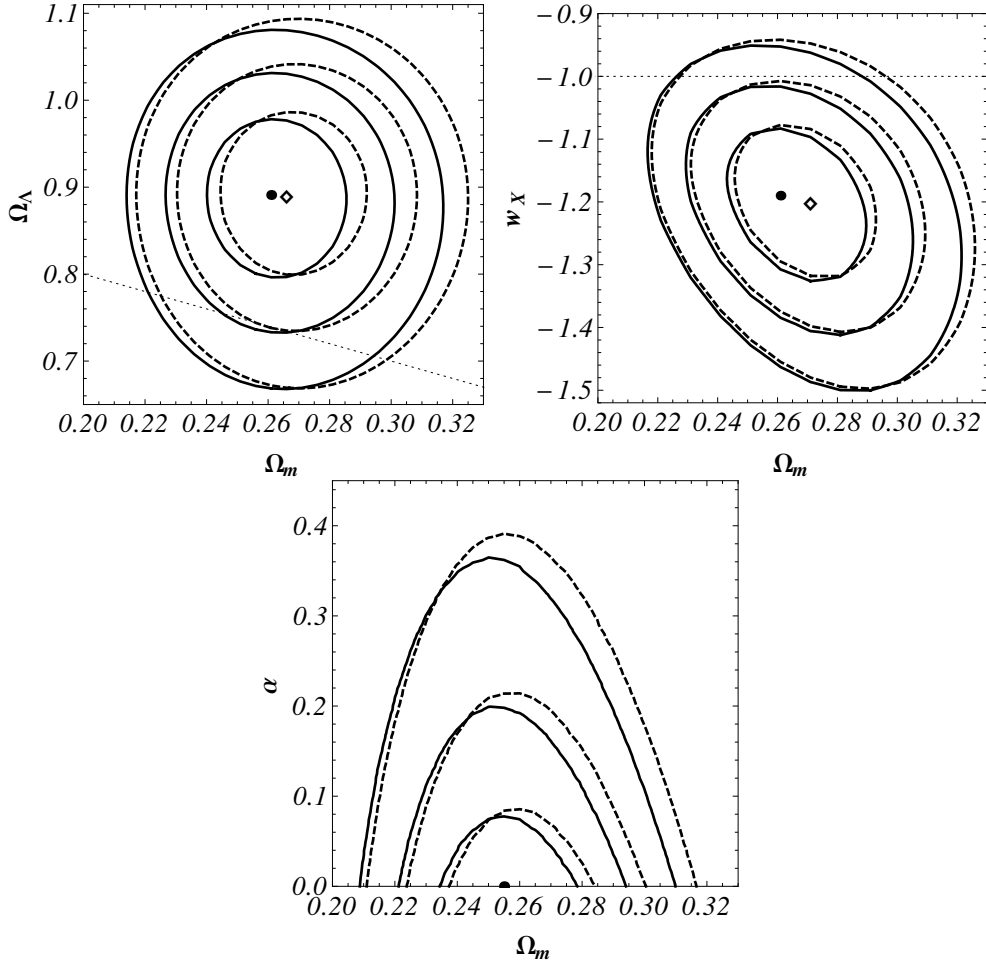
Figure 3.4: *Top left.* Joint H II galaxy, SNeIa and BAO data (solid lines) and SNeIa and BAO data (dashed lines) 1, 2, and 3σ confidence level contours in the $(\Omega_m, \Omega_\Lambda)$ plane for the ΛCDM model. The best-fit point for the first case with $-2\log(\mathcal{L}_{\max}) = 611.0$ is indicated by the solid black circle at $\Omega_m = 0.26$ and $\Omega_\Lambda = 0.89$ and for the second $-2\log(\mathcal{L}_{\max}) = 555.9$ is indicated as a diamond at $\Omega_m = 0.27$ and $\Omega_\Lambda = 0.89$.

Top right. Joint H II galaxy, SNeIa and BAO data (solid lines) and SNeIa and BAO data (dashed lines) 1, 2, and 3σ confidence level contours in the (Ω_m, w_X) plane for the spatially-flat XCDM parametrization. The best-fit point for the first case with $-2\log(\mathcal{L}_{\max}) = 609.4$ is indicated by the solid black circle at $\Omega_m = 0.26$ and $w_x = -1.19$ and for the second $-2\log(\mathcal{L}_{\max}) = 555.3$ is indicated as a diamond at $\Omega_m = 0.27$ and $w_x = -1.2$.

Bottom. Joint H II galaxy, SNeIa and BAO data (solid lines) and SNeIa and BAO data (dashed lines) 1, 2, and 3σ confidence level contours in the (Ω_m, α) plane for the spatially-flat ϕCDM model. The best-fit point for the first case with $-2\log(\mathcal{L}_{\max}) = 616.6$ and for the second $-2\log(\mathcal{L}_{\max}) = 562.0$ is indicated by the solid black circle at $\Omega_m = 0.26$ and $\alpha = 0$.
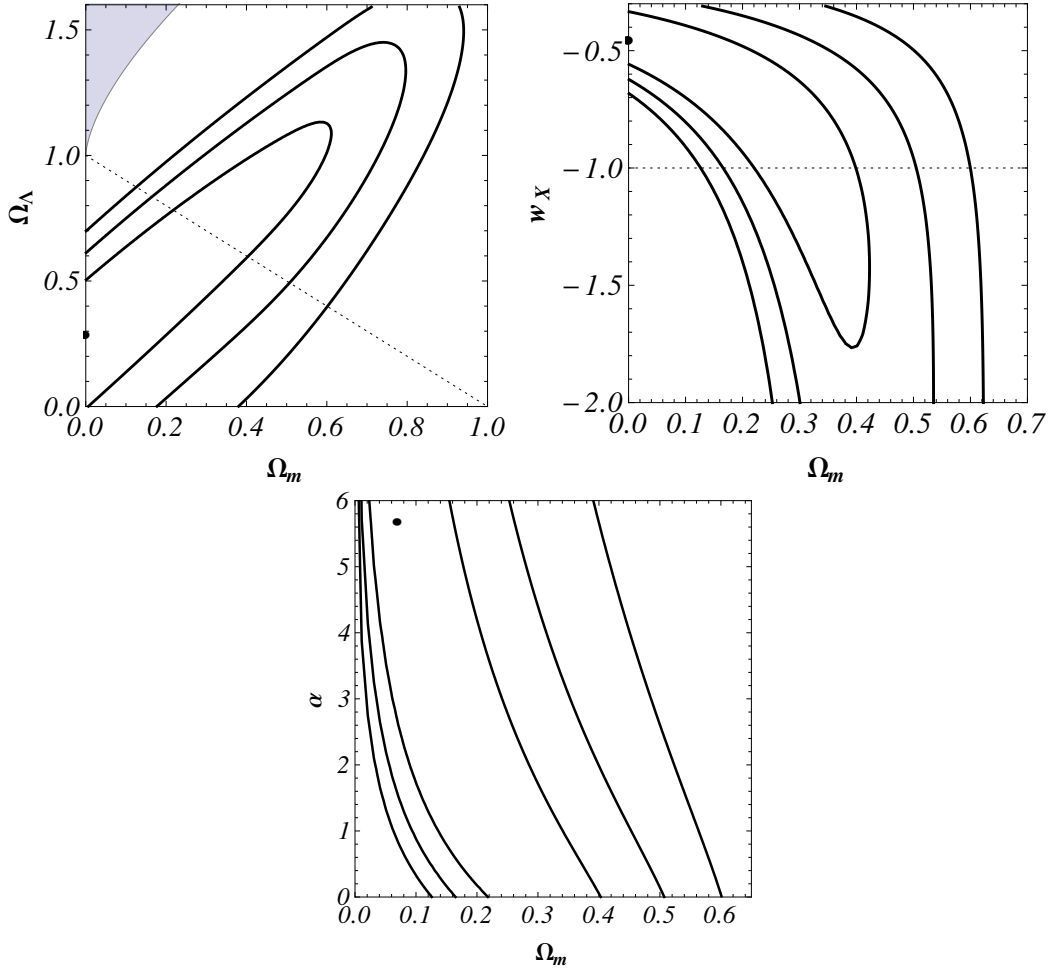
27

Figure 3.5: 3-σ contours for the ΛCDM model (*top left*), the spatially-flat XCDM parametrization (*top right*) and spatially flat ϕCDM model (*bottom*) using age-z data . In the top left panel (ΛCDM) the thin dotted diagonal line corresponds spatially-flat case and the shaded area in the upper left hand corner is the part of parameter space without a big bang, while in the left panel (XCDM) the dotted horizontal line indicates model with a time-independent cosmological constant. For ϕCDM $\alpha = 0$ corresponds spatially-flat ΛCDM case. The best-fit points are indicated by the solid black circle at $\Omega_m = 0$ and $\Omega_\Lambda = 0.27$ (*top left*), at $\Omega_m = 0$ and $w_X = -0.45$ (*top right*) and the solid black circle at $\Omega_m = 0.07$ and $\alpha = 0.57$ (*bottom*).
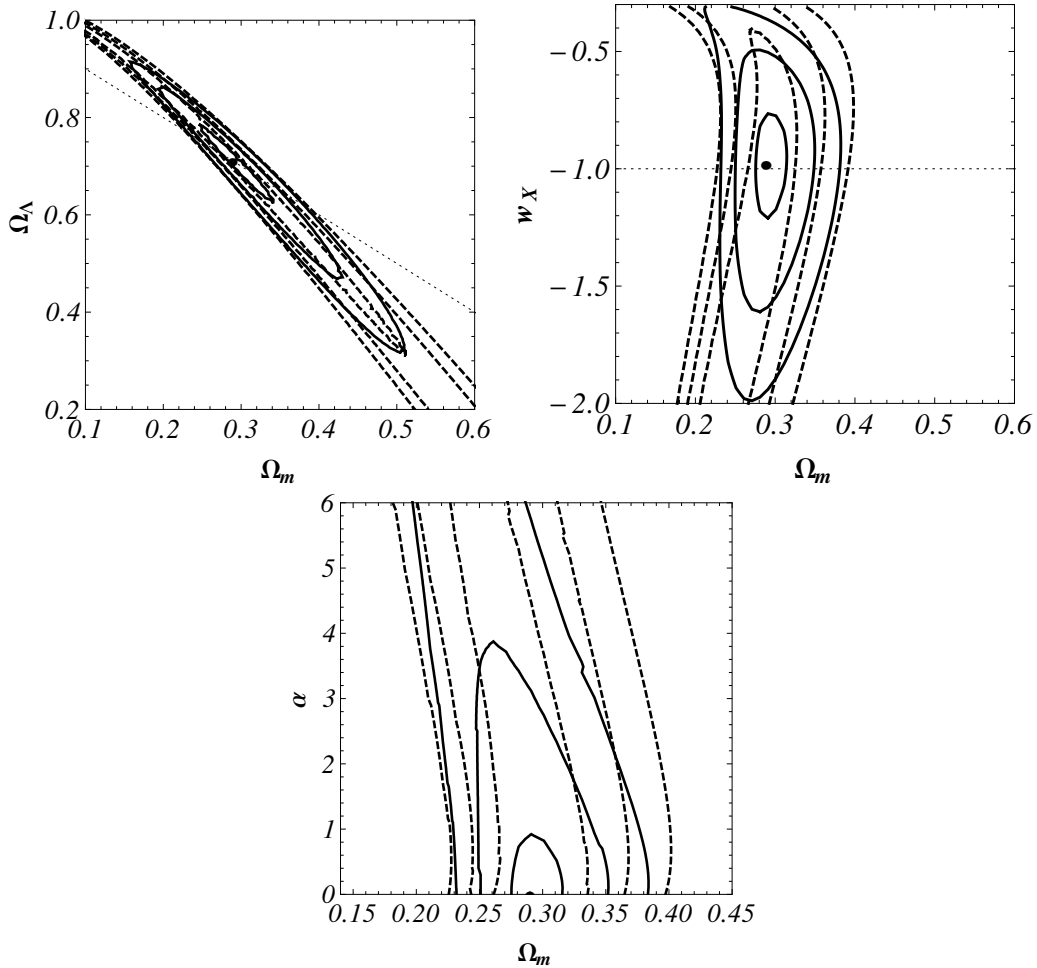
Figure 3.6: Joint age-z and BAO/CMB data constraints (solid lines) BAO/CMB only (dashed lines) 3-σ confidence level contours for the ΛCDM model (*top left*), the spatially-flat XCDM parametrization (*top right*) and spatially-flat ΛCDM (*bottom*) case. Conventions and notations are as in Fig. 3.5. The best-fit points are indicated by the solid black circle at $\Omega_m = 0.29$ and $\Omega_\Lambda = 0.71$ (*top left*), at $\Omega_m = 0.29$ and $w_X = -0.98$ (*top right*). and at $\Omega_m = 0.29$ and $\alpha = 0$ (*bottom*).

Bibliography

[1] Abraham, R. G., et al. 2004, AJ, 127, 2455

[2] Allen, S. W., et al. 2008, MNRAS, 383, 879

[3] Amanullah, R., et al. 2010, ApJ, 716, 712

[4] Astier, P., et al. 2010, arXiv:1010.0509 [astro-ph.CO]

[5] Baldi, M., & Pettorino, V. 2011, MNRAS, 412, L1

[6] Biesiada, M., Piórkowska, A., & Malec, B. 2010, MNRAS, 406, 1055

[7] Blake, C., et al. 2011, arXiv:1108.2635 [astro-ph.CO]

[8] Blanchard, A. 2010, A&A Rev., 18, 595

[9] Bonamente, M., et al. 2006, ApJ, 647, 25

[10] Brouzakis, N., et al. 2011, J. Cosmology Astropart. Phys., 1103, 049

[11] Campanelli, L., et al. 2011, arXiv:1110.2310 [astro-ph.CO]

[12] Capozziello, S., et al. 2004, Phys. Rev. D, 70, 123501

[13] Chae, K.-H., et al. 2004, ApJL, 607, L71

[14] Chen, G., & Ratra, B. 2003, ApJ, 582, 586

[15] Chen, G., & Ratra, B. 2003, PASP, 115, 1143

[16] Chen, Y., & Ratra, B. 2011, arXiv:1105.5660 [astro-ph.CO]

[17] Chen, Y., & Ratra, B. 2011, Phys. Lett. B, 703, 406

[18] Costa, F. E. M. 2010, Phys. Rev. D, 82, 103527

[19] Dantas, M. A., et al. 2007, Astron. Astrophys. 467, 421

[20] Dantas, M. A., Alcaniz, J. S., & Pires, N. 2009, Phys. Lett. B 679, 423

[21] Dantas, M. A., et al. 2011, Phys. Lett. B, 699, 239

[22] Davis, T. M., et al. 2007, ApJ, 666, 716

[23] De Boni, C., et al. 2011, MNRAS, 415, 2758

[24] de Felice, A., & Tsujikawa, S. 2010, Living Rev. Rel., 13, 3

[25] Dev, A., et al. 2008, Phys. Rev. D, 78, 083515

[26] Doran, M., Stern, S., & Thommes, E. 2007, JCAP 0704, 015

[27] Dunlop, J. S., et al. 1996, Nature, 381, 581

[28] Erb, D. K., et al. 2003, ApJ, 591, 110

[29] Erb, D. K., et al. 2006, ApJ, 646, 107

[30] Ettori, S., et al. 2009, A&A, 501, 61

[31] Farajollahi, H., et al. 2011, Ap&SS, 563

[32] Fernandez-Martinez, E., & Verde, L. 2008, J. Cosmol. Astropart. Phys., 0808, 023

[33] Gong, Y., et al. 2008, arXiv:0810.3572 [astro-ph]

[34] Guerra, E. J., Daly, R. A., & Wan, L. 2000, ApJ, 544, 659

[35] Guy, J., et al. 2010, A&A, 523, A7

[36] Harko, T., & Lobo, F. S. N. 2010, Eur. Phys. J. C, 70, 373

[37] Holsclaw, T., et al. 2010, Phys. Rev. Lett., 105, 241302

[38] Jain, B., & Khoury, J. 2010, Annals Phys., 325, 1479

[39] Jassal, H. K., Bagla, J. S., & Padmanabhan, T. 2010, MNRAS, 405, 2639

[40] Jimenez, R., et al. 2003, ApJ, 593, 622

[41] Keresztes, Z., et al. 2010, Phys. Rev. D, 82, 123534

[42] Komatsu, E., et al. 2009, ApJS, 180, 330

[43] La Vacca, G., & Bonometto, S. A.. 2011, Nucl. Phys. Proc. Suppl., 217, 68

[44] Lee, S., & Ng, K.-W. 2007, Phys. Rev. D, 76, 043518

[45] Linder, E. V. 2010, arXiv:1004.4646 [astro-ph.CO]

[46] Liu, D.-J., Wang, H., & Yang, B. 2010, Phys. Lett. B, 694, 6

[47] Liu, J., Li, M., & Zhang, X. 2011, J. Cosmology Astropart. Phys., 1106, 028

[48] Mania, D. & Ratra, B. 2011, arXiv:1110.5626 [astro-ph.CO]

[49] McCarthy, P. J., et al. 2004, ApJ, 614, L9

[50] Melnick, J. 1978, A&A, 70, 157

[51] Melnick, J. 2003, ASP Conf. Proc. Ser., 297, 3

[52] Melnick, J., Terlevich, R., & Moles, M. 1988, MNRAS, 235, 297

[53] Melnick, J., Terlevich, R., & Terlevich, E. 2000, MNRAS, 311, 629

[54] Mortonson, M. J., Hu, W., & Huterer, D. 2011, Phys. Rev. D, 83, 023015

[55] Nakamura, K., et al. (Particle Data Group) 2010, J. Phys. G: Nucl. Part. Phys. 37 075021

[56] Nolan, L. A., Dunlop, J. S., & Jimenez, R. 2001, MNRAS, 323, 385

[57] Novosyadlyj, B., et al. 2010, Phys. Rev. D, 82, 103008

[58] Pan, N., et al. 2010, Class. Quantum Grav., 27, 155015

[59] Peebles, P. J. E. 1984, ApJ, 284, 439

[60] Peebles, P. J. E. 1993, Principles of physical cosmology , (Princeton Univ Pr)

[61] Peebles, P. J. E., & Ratra, B. 1988, ApJL, 325, L17

[62] Peebles, P. J. E., & Ratra, B. 2003, Rev. Mod. Phys., 75, 559

[63] Percival, W. J., et al. 2010, MNRAS, 401, 2148

[64] Perivolaropoulos, L. 2010, J. Phys. Conf. Ser., 222, 012024

[65] Pettini, M., et al. 2001, ApJ, 554, 981

[66] Pettorino, V., et al. 2010, Phys. Rev. D, 82, 123001

[67] Pires, N., Zhu, Z.-H., & Alcaniz, J. S. 2006, Phys. Rev. D, 73, 123530

[68] Plionis, M., et al. 2010, AIP Conf. Proc. 1241, 267

[69] Plionis, M., et al. 2011, MNRAS, 416, 2981

[70] Plionis, M., et al. 2009, J. Phys. Conf. Ser., 189, 012032

[71] Podariu, S., Nugent, P., & Ratra, B. 2001, ApJ, 553, 39

[72] Podariu, S., et al. 2001, ApJ, 559, 9

[73] Podariu, S., & Ratra, B. 2000, ApJ, 532, 109

[74] Ratra, B. 1991, Phys. Rev. D, 43, 3802

[75] Ratra, B., & Peebles, P. J. E. 1988, Phys. Rev. D, 37, 3406

[76] Ratra, B., & Vogeley, M. S. 2008, PASP, 120, 235

[77] Samushia, L. 2009, PhD thesis, arXiv:0908.4597 [astro-ph.CO]

[78] Samushia, L., Chen, G., & Ratra, B. 2007, arXiv:0706.1963 [astro-ph]

[79] Samushia, L., et al. 2010, Phys. Lett. B, 693, 509

[80] Samushia, L., & Ratra, B. 2006, ApJL, 650, L5

[81] Samushia, L., & Ratra, B. 2008, ApJL, 680, L1

[82] Samushia, L., & Ratra, B. 2009, ApJ, 701, 1373

[83] Samushia, L., & Ratra, B. 2010, ApJ, 714, 1347

[84] Samushia, L., et al. 2011, MNRAS, 410, 1993

[85] Sanderson, C. 2010, Tech. rep., NICTA

[86] Sapone, D. 2010, Int. J. Mod. Phys. A, 25, 5253

[87] Schaefer, B. E. 2007, ApJ, 660, 16

[88] Sen, A. A., & Scherrer, R. J. 2008, Phys. Lett. B, 659, 457

[89] Siegel, E. R., et al. 2005, MNRAS, 356, 1117

[90] Simon, J., Verde, L., & Jimenez, R. 2005, Phys. Rev. D 71, 123001.

[91] Sollerman, J. et al. 2009, ApJ, 703, 1374.

[92] Spinrad, H., et al. 1997, ApJ, 484, 581

[93] Suzuki, N., et al. 2012, ApJ, 746, 85

[94] Terlevich, R., & Melnick, J. 1981, MNRAS, 195, 839

[95] Terlevich, E., Terlevich, R., & Melnick, J. 2002, Rev. Mex. A&A (Ser. Conf.), 12, 272

[96] Tong, M., & Noh, H. 2011, Eur. Phys. J. C, 71, 1586

[97] Treu, T., et al. 1999, MNRAS, 308, 1037

[98] Treu, T., et al. 2001, MNRAS, 326, 221

[99] Treu, T., et al. 2002, ApJ, 564, L13

[100] Tsujikawa, S. 2010, arXiv:1004.1493 [astro-ph.CO]

[101] Wang, S., Li, X.-D., & Li, M. 2011, Phys. Rev. D, 83, 023010

[102] Wang, Y. 2008, Phys. Rev. D, 78, 123532

[103] Wang, Y. 2010, Mod. Phys. Lett. A, 25, 3093

[104] Wang, Y., et al. 2010, MNRAS, 409, 737

[105] Wei, H. 2009, Nucl. Phys. B, 819, 210

[106] Wilson, K. M., Chen, G., & Ratra, B. 2006, Mod. Phys. Lett. A, 21, 2197

[107] Xu, L., & Wang, Y. 2010, J. Cosmology Astropart. Phys., 1011, 014

[108] Yang, R.-J., & Zhang, S. N. 2009, arXiv:0905.2683 [astro-ph.CO]

[109] Zhang, Q.-J., & Wu, Y.-L. 2010, J. Cosmology Astropart. Phys., 1008, 038

Appendix A

Derivation of Scalar Field equation of motion

General scalar field action in Riemann metric can be written as:

$$S = \int d^4x \sqrt{-g} \mathcal{L}(\partial_\mu \phi, \phi)$$

Satisfying Euler-Lagrange equations:

$$\partial_\mu \frac{\partial(\sqrt{-g}\mathcal{L})}{\partial(\partial_\mu \phi)} - \frac{\partial(\sqrt{-g}\mathcal{L})}{\partial \phi} = 0$$

In ϕCDM case Lagrangian has the form[75]:

$$\mathcal{L} = \frac{1}{32\pi G} \left(g^{\mu\nu} \partial_\mu \phi \partial_\nu \phi - \kappa m_p^2 \phi^{-\alpha} \right)$$

Putting in Euler-Lagrange equations:

$$\partial_\mu(\sqrt{-g}g^{\mu\nu}\partial_\nu \phi) - \sqrt{-g}\frac{\kappa m_p^2 \alpha}{2}\phi^{-(\alpha+1)} = 0$$

$$\frac{1}{2g}\partial_\mu g g^{\mu\nu}\partial_\nu \phi + \partial_\mu g^{\mu\nu}\partial_\nu \phi + g^{\mu\nu}\partial_\mu \partial_\nu \phi - \frac{\kappa m_p^2 \alpha}{2}\phi^{-(\alpha+1)} = 0$$

Using the FLRW metric 1.1

$$g^{\mu\nu} = \begin{pmatrix} 1 & 0 & 0 & 0 \\ 0 & -a^2(t) & 0 & 0 \\ 0 & 0 & -a^2(t) & 0 \\ 0 & 0 & 0 & -a^2(t) \end{pmatrix}$$

We can calculate

$$g = -a^6(t), \ \phi = \phi(t)$$

$$\partial_i \phi = 0, \ \partial_i g^{\mu\nu} = 0, \ \partial_0 g^{00} = 0$$

$$\partial_0 g = -6a^5 \dot{a}$$

resulting the equation of motion for ϕ field.

$$3\frac{\dot{a}}{a}\dot{\phi} + \ddot{\phi} - \frac{\kappa m_p^2 \alpha}{2}\phi^{-(\alpha+1)} = 0$$